https://doi.org/10.20965/jrm.2017.p0500

Paper:

Visual Lifting Approach for Bipedal Walking with Slippage

Xiang Li, Mamoru Minami, Takayuki Matsuno, and Daiji Izawa

Graduate School of Nature Science and Technology, Okayama University
3-1-1 Tsushima-naka, Kita-ku, Okayama-shi, Okayama 700-8530, Japan
E-mail: pzkm87r2@s.okayama-u.ac.jp
[Received January 24, 2017; accepted March 13, 2017]

Biped locomotion generated by control methods based on Zero-Moment Point (ZMP) has been achieved and its efficacy for stable walking, where ZMP-based walking does not include the falling state, has been verified extensively. The walking control that does not depend on ZMP – we call it dynamical walking – can be used in walking that utilizes kicks by toes, which looks natural but is vulnerable to turnover. Therefore, keeping the walking of dynamical motion stable is indispensable to the realization of human-like natural walking – the authors perceive the human walking, which includes toe off states, as natural walking. Our research group has developed a walking model, which includes slipping, impact, surface-contacting and line-contacting of foot. This model was derived from the Newton-Euler (NE) method. The "Visual Lifting Approach" (VLA) strategy inspired from human walking motion utilizing visual perception, was used in order to enhance robust walking and prevent the robot from falling, without utilizing ZMP. The VLA consists of walking gate generation visual lifting feedback and feedforward. In this study, simulation results confirmed that bipedal walking dynamics, which include a slipping state between foot and floor, converge to a stable walking limit cycle.

Keywords: humanoid, bipedal walking, visual lifting approach

1. Introduction

With regard to humanoid walking control, ZMP-based walking is considered the most promising approach and it has been confirmed as a realistic control strategy for achieving the stable walking of actual biped robots. This is possible because ZMP-based walking can guarantee that the robots are able to maintain a standing position by retaining the ZMP within the convex hull of the supporting area [1, 2]. However, the walking profile of the ZMP-based strategy looks waist-lowered, similar to the walking style of monkeys. As alternatives to the ZMP, other approaches have focused on keeping the robot's walking trajectories inside a basin of attraction [3–5], including a method that refers to the limit cycle in order to determine the input torque [6].

Previous discussions were based on simplified bipedal models, which tend to avoid the consideration of slipping or the real world effects of feet. Contrary to the above, Huang et al. (2010) [7] pointed out that the effect of feet accounts for different varieties of walking gait, e.g., point contacting (heel contacting) and surface contacting (foot-sole ground contact), causing the dimensional change of state variables. Our research started out with a point of view similar to the one held by Huang et al. (2010) [7]. Thereby, our initial purpose was to describe gait dynamics as accurately as possible, including the foot's point/surface-contact state, foot slipping and bumping, where the walking gait transition would be decided with regard to walking motion. This is called event-driven transition [8]. The model used by Huang et al. (2010) [7] does not account for the body, arms and head. Therefore, it is different from our model, which includes whole-body dynamics and accounts for arms and head. Importance is placed on dimension of the motion equation, which changes depending on the particular walking gait variety, introduced by Wu et al. (2010) [9] which considers a one-legged hopping robot.

If we consider the example of the heel being detached from the ground while the toe is in contact, a new state variable describing the foot's rotation would emerge. This would result to the increase of a number of state variables. In fact, this kind of dynamics with the state dimension number being changed by the result of its dynamical time motion profiles are out of the scope of control theory, which is concerned with how to control a system that has a fixed number of states. Further, tipping over motion, known as non-holonomic dynamics, includes a joint without inputting torque, i.e., a free joint.

Additionally, the landing of the lifted toe's heel or toe on the ground makes geometrical contact. Nakamura and Yamane (2000) [10] described how to represent contact with an environment that can handle constraint motion with friction, using algebraic equations, and applied it to human figures [11]. On the basis of these references, 20 kinds of gait dynamics were derived, including slipping motion with both varying constraint conditions and dimensional changing of state variables. As a result, the dynamical model was elaborated as much as possible [12].

In our previous work on the VLA [13–15], an incomplete humanoid model was used, in which the head, arms

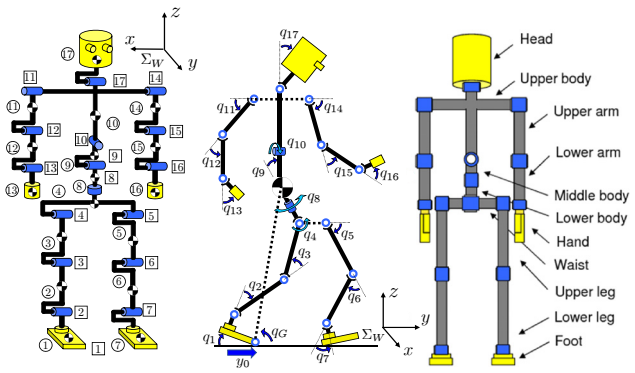

Fig. 1. Definition of humanoid's link, joint and whole body, ①–⑰ represents link number, 1 – 17 means joint number, q_1–q_{17} means joint angles.

Table 1. Physical parameters.

Link	l_i [m]	m_i [kg]	d_i [Nms/rad]
Head	0.24	4.5	0.5
Upper body	0.41	21.5	10.0
Middle body	0.1	2.0	10.0
Lower body	0.1	2.0	10.0
Upper arm	0.31	2.3	0.03
Lower arm	0.24	1.4	1.0
Hand	0.18	0.4	2.0
Waist	0.27	2.0	10.0
Upper leg	0.38	7.3	10.0
Lower leg	0.40	3.4	10.0
Foot	0.07	1.3	10.0
Total weight [kg]	—	64.2	—
Total hight [m]	1.7	—	—

and torso, were omitted. Therefore, the model was too simple, since the effect of the arm and upper body's dynamical coupling were not considered. However, an improved model was used in the present study which considers slipping in the sagittal direction. The validity of the model was verified and the results were presented recently in a published paper [12].

In this study, we investigated the potential of ZMP-independent walking in realizing human-like natural walking with slippage, including the toe-off state. The "Visual Lifting Approach" (VLA) based on the visual servoing and visual feedback concepts, which are in turn based on the similar concept of impedance control [16], was used. A real-time pose tracking method has been proposed, as a visual pose estimation [17, 18] by which a 3D object, set near the humanoid, measures the robot's head relative to position and orientation. The simulation results showed that visual feedback helped realize stable bipedal walking and that ZMP exists on the convex hull boundary line of the supporting area, under the condition that humanoid dynamics include toe-off, slipping and bumping. Furthermore, this paper discusses the effectiveness of the VLA in making bipedal walking dynamics, including the slipping state between the foot and floor, converge to stable walking limit cycles.

2. Dynamical Walking Model

2.1. Forward Kinematical Calculations

In this paper, a biped robot, whose definition is depicted in **Fig. 1**, is discussed. **Table 1** indicates the length l_i [m], mass m_i [kg] of links and the coefficient of the joints' viscous friction d_i [N·m·s/rad], which were decided based on the study by Kouchi et al. (2000) [19]. This model was simulated as a serial-link manipulator with ramifications on both of waist and upper body and represented the rigid whole body – feet including toe, torso, arms and so on – with 17 degree-of-freedom. Although the motion of legs is restricted in the sagittal plane, the model generates various walking gait sequences, since the robot has flat-sole feet and kicking torque. In this paper, the foot called link-1 is defined the "supporting-foot" and the other foot, called link-7, is defined as the "free-foot" ("contacting-foot" when the free-foot makes contact with the floor) according to the walking state. When the slipping of the contacting-foot stopped, meaning that static friction force was exerted to the foot, the contacting-foot was transferred into the supporting-foot and the previously supporting-foot changed to being the free-foot when it was detached from ground.

The motion equation was derived by following the NE formulation [19, 20]; therefore, the structure of the supporting-foot needed to be considered in two situations. When the supporting-foot was constituted by a rotating joint, the relations of positions made by rotation were first calculated, followed by the velocities and accelerations between links, as forward kinematics procedures from the bottom link to the top link. The serial link's angular velocity ${}^i\boldsymbol{\omega}_i$, angular acceleration ${}^i\dot{\boldsymbol{\omega}}_i$, acceleration of the origin ${}^i\ddot{\boldsymbol{p}}_i$ and acceleration of the center of mass ${}^i\ddot{\boldsymbol{s}}_i$ based on Σ_i fixed at the i-th link, which included the supporting-foot being rotational, were obtained as follows:

$$ {}^i\boldsymbol{\omega}_i = {}^{i-1}\boldsymbol{R}_i^T\, {}^{i-1}\boldsymbol{\omega}_{i-1} + \boldsymbol{e}_{z_i}\dot{q}_i \quad . . . . . \quad (1) $$

$$ {}^i\dot{\boldsymbol{\omega}}_i = {}^{i-1}\boldsymbol{R}_i^T\, {}^{i-1}\dot{\boldsymbol{\omega}}_{i-1} + \boldsymbol{e}_{z_i}\ddot{q}_i + {}^i\boldsymbol{\omega}_i \times (\boldsymbol{e}_{z_i}\dot{q}_i) \quad . \quad (2) $$

$$ {}^i\ddot{\boldsymbol{p}}_i = {}^{i-1}\boldsymbol{R}_i^T \Big\{ {}^{i-1}\ddot{\boldsymbol{p}}_{i-1} + {}^{i-1}\dot{\boldsymbol{\omega}}_{i-1} \times {}^{i-1}\hat{\boldsymbol{p}}_i + {}^{i-1}\boldsymbol{\omega}_{i-1} \times ({}^{i-1}\boldsymbol{\omega}_{i-1} \times {}^{i-1}\hat{\boldsymbol{p}}_i) \Big\} \quad (3) $$

$$ {}^i\ddot{\boldsymbol{s}}_i = {}^i\ddot{\boldsymbol{p}}_i + {}^i\dot{\boldsymbol{\omega}}_i \times {}^i\hat{\boldsymbol{s}}_i + {}^i\boldsymbol{\omega}_i \times ({}^i\boldsymbol{\omega}_i \times {}^i\hat{\boldsymbol{s}}_i). \quad . \quad (4) $$

Here, ${}^{i-1}\boldsymbol{R}_i$ means orientation matrix, ${}^{i-1}\hat{\boldsymbol{p}}_i$ represents the position vector from the origin of $(i-1)$-th link to the one of i-th, ${}^i\hat{\boldsymbol{s}}_i$ is defined as gravity center position of i-th link and $\boldsymbol{e}_{z_i}$ is a unit vector, which shows the rotational axis of i-th link.

If the supporting-foot is slipping, it should be described as a prismatic joint, which is used in the modeling of foot

slippage. The equations will then switch as follows:

$$ {}^{i}\boldsymbol{\omega}_i = {}^{i-1}\boldsymbol{R}_i^{\mathrm{T}}\,{}^{i-1}\boldsymbol{\omega}_{i-1} \quad (5)$$

$$ {}^{i}\dot{\boldsymbol{\omega}}_i = {}^{i-1}\boldsymbol{R}_i^{\mathrm{T}}\,{}^{i-1}\dot{\boldsymbol{\omega}}_{i-1} \quad (6)$$

$$ \begin{aligned} {}^{i}\ddot{\boldsymbol{p}}_i = {}^{i-1}\boldsymbol{R}_i^{\mathrm{T}}\Big\{ &{}^{i-1}\ddot{\boldsymbol{p}}_{i-1} + {}^{i-1}\dot{\boldsymbol{\omega}}_{i-1} \times {}^{i-1}\hat{\boldsymbol{p}}_i \\ &+ {}^{i-1}\boldsymbol{\omega}_{i-1} \times ({}^{i-1}\boldsymbol{\omega}_{i-1} \times {}^{i-1}\hat{\boldsymbol{p}}_i)\Big\} \\ &+ 2({}^{i-1}\boldsymbol{R}_i^{T\,i-1}\boldsymbol{\omega}_{i-1}) \times (\boldsymbol{e}_{zi}\dot{q}_i) + \boldsymbol{e}_{zi}\ddot{q}_i \end{aligned} \quad (7)$$

$$ {}^{i}\ddot{\boldsymbol{s}}_i = {}^{i}\ddot{\boldsymbol{p}}_i + {}^{i}\dot{\boldsymbol{\omega}}_i \times {}^{i}\hat{\boldsymbol{s}}_i + {}^{i}\boldsymbol{\omega}_i \times ({}^{i}\boldsymbol{\omega}_i \times {}^{i}\hat{\boldsymbol{s}}_i) \quad (8)$$

where in this case, $\boldsymbol{e}_{zi}$ represents the slipping direction.

The velocity and acceleration of the 4th link are transmitted to the 5th and 8th link and the ones of the 10th link are transmitted to the 11th, 14th and 17th links directly, due to ramification mechanisms, as shown in **Fig. 1**.

2.2. Backward Inverse Dynamical Calculations

After the above forward kinematic calculation was carried out, contrarily inverse dynamical calculation from the top to the base link was required as shown below. The Newton and Euler equations of the i-th link are represented by Eqs. (9) and (10) where ${}^{i}\boldsymbol{I}_i$ is defined as the inertia tensor of the i-th link. Here, ${}^{i}\boldsymbol{f}_i$ and ${}^{i}\boldsymbol{n}_i$ in Σ_i show the force and moment exerted on the i-th link from the $(i+1)$-th link based on the coordinates of Σ_i.

$$ {}^{i}\boldsymbol{f}_i = {}^{i}\boldsymbol{R}_{i+1}{}^{i+1}\boldsymbol{f}_{i+1} + m_i{}^{i}\ddot{\boldsymbol{s}}_i \quad (9)$$

$$ \begin{aligned} {}^{i}\boldsymbol{n}_i = &{}^{i}\boldsymbol{R}_{i+1}{}^{i+1}\boldsymbol{f}_{i+1} + {}^{i}\boldsymbol{I}_i{}^{i}\dot{\boldsymbol{\omega}}_i + {}^{i}\boldsymbol{\omega}_i \times ({}^{i}\boldsymbol{I}_i{}^{i}\boldsymbol{\omega}_i) \\ &+ {}^{i}\hat{\boldsymbol{s}}_i \times (m_i{}^{i}\ddot{\boldsymbol{s}}_i) + {}^{i}\hat{\boldsymbol{p}}_{i+1} \times ({}^{i}\boldsymbol{R}_{i+1}{}^{i+1}\boldsymbol{f}_{i+1}) \end{aligned} \quad (10)$$

On the other hand, since force and torque of the 5th and the 8th links are exerted on the 4th link, effects onto the 4th link are described as:

$$ {}^{4}\boldsymbol{f}_4 = {}^{4}\boldsymbol{R}_5{}^{5}\boldsymbol{f}_5 + {}^{4}\boldsymbol{R}_8{}^{8}\boldsymbol{f}_8 + m_4{}^{4}\ddot{\boldsymbol{s}}_4, \quad (11)$$

$$ \begin{aligned} {}^{4}\boldsymbol{n}_4 = &{}^{4}\boldsymbol{R}_5{}^{5}\boldsymbol{n}_5 + {}^{4}\boldsymbol{R}_8{}^{8}\boldsymbol{n}_8 + {}^{4}\boldsymbol{I}_4{}^{4}\dot{\boldsymbol{\omega}}_4 + {}^{4}\boldsymbol{\omega}_4 \times ({}^{4}\boldsymbol{I}_4{}^{4}\boldsymbol{\omega}_4) \\ &+ {}^{4}\hat{\boldsymbol{s}}_4 \times (m_4{}^{4}\ddot{\boldsymbol{s}}_4) + {}^{4}\hat{\boldsymbol{p}}_5 \times ({}^{4}\boldsymbol{R}_5{}^{5}\boldsymbol{f}_5) \\ &+ {}^{4}\hat{\boldsymbol{p}}_8 \times ({}^{4}\boldsymbol{R}_8{}^{8}\boldsymbol{f}_8). \end{aligned} \quad (12)$$

Similarly, the force and torque of the 11th, 14th and 17th links are transmitted to the 10th link directly. Then, the inverse calculation of i-th link, which is equivalent to rotational equation of motion of the i-th link, is obtained as Eq. (13) by making the inner product of the induced torque onto the i-th link's unit vector $\boldsymbol{e}_{z_i}$ around the rotational axis:

$$ \tau_i = \boldsymbol{e}_{z_i}^{T}\,{}^{i}\boldsymbol{n}_i + d_i\dot{q}_i. \quad (13)$$

However, when the supporting-foot (1st link) is slipping (prismatic joint), the force exerted onto the 1st link may be calculated by the following equation:

$$ f_{y_0} = \boldsymbol{e}_{z_0}^{T}\,{}^{0}\boldsymbol{f}_0 + \mu_k\dot{y}_0. \quad (14)$$

where $\dot{y}_0$ represents the slipping velocity.

Finally, the motion equation, when one foot is standing, can be derived as:

$$ \boldsymbol{M}(\boldsymbol{q})\ddot{\boldsymbol{q}} + \boldsymbol{h}(\boldsymbol{q},\dot{\boldsymbol{q}}) + \boldsymbol{g}(\boldsymbol{q}) + \boldsymbol{D}\dot{\boldsymbol{q}} = \boldsymbol{\tau}. \quad (15)$$

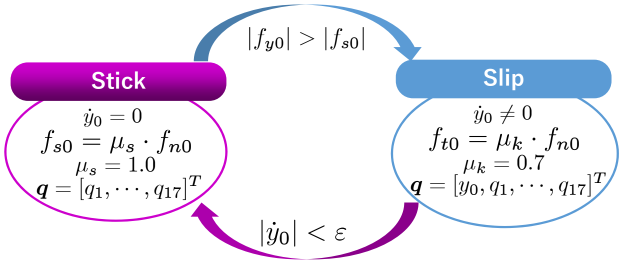

Fig. 2. Switch conditions of stick-slip motion.

Here, $\boldsymbol{\tau} = [f_{y_0}, \tau_1, \tau_2, \ldots, \tau_{17}]$ is the input torque, where f_0 is always identical to zero since the slipping motion does not have an actuator. $\boldsymbol{M}(\boldsymbol{q})$ is the inertia matrix, $\boldsymbol{h}(\boldsymbol{q},\dot{\boldsymbol{q}})$ are vectors that indicate the Coriolis force and centrifugal forces, and $\boldsymbol{g}(\boldsymbol{q})$ represents the gravity force. μ_k in $\boldsymbol{D} = diag[\mu_k,\, d_1,\, d_2,\, \ldots,\, d_{17}]$ is the coefficient of friction, μ_k is the friction coefficient between foot and ground. In addition $\boldsymbol{q} = [y_0,\ q_1,\ q_2,\ \ldots,\ q_{17}]^T$ represents the relative position y_0 between foot and ground, which is generated by the slipping and angle of joints q_1–q_{17}. The viscous friction force of the y-axis (slipping axis) can be expressed as $\mu_k\dot{y}_0$, which is included in the left-hand side of Eq. (15).

This slipping motion state is depicted at the right side of **Fig. 2**. If $|\dot{y}_0| < \varepsilon$ is satisfied, the degree of motion y_0 disappears; then the motion equation transfers to the motion equation consisting of $\boldsymbol{q} = [q_1, q_2, \ldots, q_{17}]^T$. In this state, the static friction coefficient $\mu_s = 1.0$ is applied, and static friction force $f_{s0} = \mu_s f_{n0}$ is exerted to the lateral direction of the foot. When the exerting lateral force f_{y0} is generated by the dynamical coupling of the humanoid body calculated by Eq. (14), it should satisfy $|f_{y0}| > |f_{s0}|$. At that point, slipping motion starts and the motion equation, which includes $\boldsymbol{q} = [q_1,\ q_2,\ \ldots,\ q_{17}]^T$, is changed to the motion equation with variables of $\boldsymbol{q} = [y_0,\ q_1,\ q_2,\ \ldots,\ q_{17}]^T$ again, as depicted in the right state shown in **Fig. 2**.

2.3. Free-Foot Constraint Conditions

When making free-foot contact with the ground, the free-foot appears to have the foot position as zero and the angle of foot to the ground is constrained to zero. In addition, when the velocity of the free-foot in the traveling direction $\dot{y}_0$ is less than 0.0002 mm/Δt ($\Delta t = 2 \times 10^{-4}$ s, which is the Runge-Kutta integration period), the free-foot can be considered to have stopped and constrained by static friction. The constraints of the foot's z-axis heel position and rotation and the foot's y-axis position, based on the coordinates of Σ_W in **Fig. 1**, can be defined as C_1, C_2 and C_3, respectively. These constraints can be written as shown below:

$$ \boldsymbol{C}(\boldsymbol{r}(\boldsymbol{q})) = \begin{bmatrix} C_1(\boldsymbol{r}(\boldsymbol{q})) \\ C_2(\boldsymbol{r}(\boldsymbol{q})) \\ C_3(\boldsymbol{r}(\boldsymbol{q})) \end{bmatrix} = \boldsymbol{0} \quad (16)$$

where $\boldsymbol{r}(\boldsymbol{q})$ means the free-foot's heel or toe position in Σ_W.

Then, the robot's motion equation with external force f_{nz}, friction force f_t, external torque τ_n and external force f_{ny} generated as static friction forces corresponding to C_1, C_2 and C_3, respectively, can be derived as:

$$\begin{aligned}\boldsymbol{M}(\boldsymbol{q})\ddot{\boldsymbol{q}}+\boldsymbol{h}(\boldsymbol{q},\dot{\boldsymbol{q}})+\boldsymbol{g}(\boldsymbol{q})+\boldsymbol{D}\dot{\boldsymbol{q}}\\ =\boldsymbol{\tau}+\boldsymbol{j}_{cz}^T f_{nz}-\boldsymbol{j}_t^T f_t+\boldsymbol{j}_r^T\tau_n+\boldsymbol{j}_{cy}^T f_{ny}\end{aligned} \quad . \quad (17)$$

where $\boldsymbol{j}_{cz}$, $\boldsymbol{j}_t$, $\boldsymbol{j}_r$ and $\boldsymbol{j}_{cy}$ are defined as:

$$\boldsymbol{j}_{cz}^T=\left(\frac{\partial C_1}{\partial \boldsymbol{q}^T}\right)^T\left(\frac{1}{\left\|\frac{\partial C_1}{\partial \boldsymbol{r}^T}\right\|}\right),\quad \boldsymbol{j}_t^T=\left(\frac{\partial \boldsymbol{r}}{\partial \boldsymbol{q}^T}\right)^T\frac{\dot{\boldsymbol{r}}}{\|\dot{\boldsymbol{r}}\|},$$

$$\boldsymbol{j}_r^T=\left(\frac{\partial C_2}{\partial \boldsymbol{q}^T}\right)^T\left(\frac{1}{\left\|\frac{\partial C_2}{\partial \boldsymbol{q}^T}\right\|}\right),\quad \boldsymbol{j}_{cy}^T=\left(\frac{\partial C_3}{\partial \boldsymbol{q}^T}\right)^T\left(\frac{1}{\left\|\frac{\partial C_3}{\partial \boldsymbol{q}^T}\right\|}\right). \quad . \quad (18)$$

It is common sense that (i) f_{nz} and f_t are orthogonal, and that (ii) the value of f_t is decided by $f_t=Kf_{nz}$ $(0<K\leq 1)$. By differentiating Eq. (16) twice with respect to time, the constraint condition of $\ddot{\boldsymbol{q}}$ can be derived as follows:

$$\left(\frac{\partial C_i}{\partial \boldsymbol{q}^T}\right)\ddot{\boldsymbol{q}}+\dot{\boldsymbol{q}}^T\left\{\frac{\partial}{\partial \boldsymbol{q}}\left(\frac{\partial C_i}{\partial \boldsymbol{q}^T}\right)\right\}\dot{\boldsymbol{q}}=0 \quad (i=1,\ 2,\ 3) \quad (19)$$

By making $\ddot{\boldsymbol{q}}$ in Eqs. (17) and (19) identical, the equation of contacting motion can then be obtained as follows:

$$\begin{aligned}&\begin{bmatrix}\boldsymbol{M}(\boldsymbol{q}) & -(\boldsymbol{j}_{cz}^T-\boldsymbol{j}_t^T K) & -\boldsymbol{j}_r^T & -\boldsymbol{j}_{cy}^T\\ \frac{\partial C_1}{\partial \boldsymbol{q}^T} & 0 & 0 & 0\\ \frac{\partial C_2}{\partial \boldsymbol{q}^T} & 0 & 0 & 0\\ \frac{\partial C_3}{\partial \boldsymbol{q}^T} & 0 & 0 & 0\end{bmatrix}\begin{bmatrix}\ddot{\boldsymbol{q}}\\ f_{nz}\\ \tau_n\\ f_{ny}\end{bmatrix}\\ &=\begin{bmatrix}\boldsymbol{\tau}-\boldsymbol{h}(\boldsymbol{q},\dot{\boldsymbol{q}})-\boldsymbol{g}(\boldsymbol{q})-\boldsymbol{D}\dot{\boldsymbol{q}}\\ -\dot{\boldsymbol{q}}^T\left\{\frac{\partial}{\partial \boldsymbol{q}}\left(\frac{\partial C_1}{\partial \boldsymbol{q}^T}\right)\right\}\dot{\boldsymbol{q}}\\ -\dot{\boldsymbol{q}}^T\left\{\frac{\partial}{\partial \boldsymbol{q}}\left(\frac{\partial C_2}{\partial \boldsymbol{q}^T}\right)\right\}\dot{\boldsymbol{q}}\\ -\dot{\boldsymbol{q}}^T\left\{\frac{\partial}{\partial \boldsymbol{q}}\left(\frac{\partial C_3}{\partial \boldsymbol{q}^T}\right)\right\}\dot{\boldsymbol{q}}\end{bmatrix}.\end{aligned} \quad . \quad (20)$$

2.4. Bumping Calculation

When the swing-foot touches the ground, the treatment of bumping motion needs to be considered. There are two kinds of bumping, which concern the heel and toe. The dynamics of bumping between the heel and the ground are shown below. By integrating Eq. (17) under $\tau_n=0$ in time, under reasonable assumptions, the equation of striking moment can then be obtained as follow:

$$\boldsymbol{M}(\boldsymbol{q})\dot{\boldsymbol{q}}(t_1^+)=\boldsymbol{M}(\boldsymbol{q})\dot{\boldsymbol{q}}(t_1^-)+(\boldsymbol{j}_c^T-\boldsymbol{j}_t^T K)F_{im}. \quad (21)$$

Eq. (21) describes the bumping of Σ_W in the z-axis between the heel and the ground. $\dot{\boldsymbol{q}}(t_1^+)$ and $\dot{\boldsymbol{q}}(t_1^-)$ are the angular velocity after and before the striking respectively. The impulse of bumping, F_{im}, can be defined as:

$$F_{im}=\lim_{t_1^-\to t_1^+}\int_{t_1^-}^{t_1^+} f_{nz}dt. \quad . \quad (22)$$

The velocity of the robot is constrained by the following equation, which is given by differentiating C_1 with respect to time after the strike:

$$\frac{\partial C_1}{\partial \boldsymbol{q}}\dot{\boldsymbol{q}}(t_1^+)=0. \quad . \quad (23)$$

Then, the matrix formation equation in the case of heel's bumping can be obtained as shown below. The velocity $\dot{\boldsymbol{q}}(t_1^+)$, after the bumping, is calculated by using the inverse matrix at the left-hand side of Eq. (24).

$$\begin{aligned}&\begin{bmatrix}\boldsymbol{M}(\boldsymbol{q}) & -(\boldsymbol{j}_{cz}^T-\boldsymbol{j}_t^T K)\\ \frac{\partial C_1}{\partial \boldsymbol{q}^T} & 0\end{bmatrix}\begin{bmatrix}\dot{\boldsymbol{q}}(t_1^+)\\ F_{im}\end{bmatrix}\\ &=\begin{bmatrix}\boldsymbol{M}(\boldsymbol{q})\dot{\boldsymbol{q}}(t_1^-)\\ 0\end{bmatrix}.\end{aligned} \quad . \quad (24)$$

The dynamics of the toe's bumping can be derived by a process similar to the above.

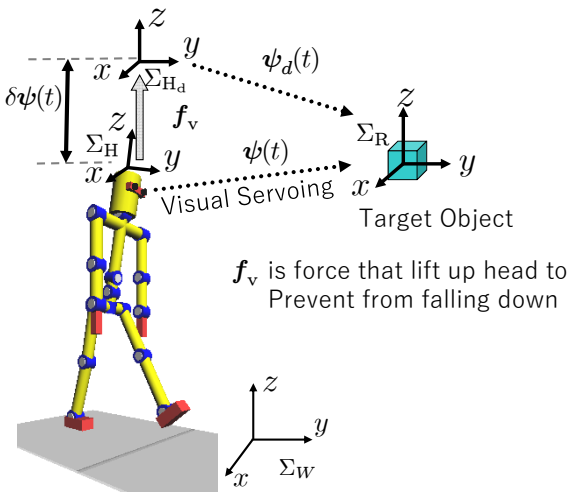

Fig. 3. Concept of visual lifting approach.

3. Visual Lifting Approach

3.1. Feedback Lifting Torque Generator

This section describes the VLA, which is a visual-feedback control for improving humanoid standing and walking stability as shown in **Fig. 3**. The model-based matching method is used to measure the relative pose $\boldsymbol{\psi}(t)$ between a stationary target object and the head rep-

resented by Σ_H in Σ_W. The desired relative pose of Σ_R (reference target object's coordinate) and Σ_H is predefined by homogeneous transformation as ${}^H\boldsymbol{T}_R$. The difference between the desired head pose Σ_{Hd} and the current pose Σ_H is denoted as ${}^H\boldsymbol{T}_{Hd}$ and can be described by:

$$ {}^H\boldsymbol{T}_{H_d}(\boldsymbol{\psi}_d(t), \boldsymbol{\psi}(t)) = {}^H\boldsymbol{T}_R(\boldsymbol{\psi}(t)) \cdot {}^{H_d}\boldsymbol{T}_R{}^{-1}(\boldsymbol{\psi}_{\boldsymbol{d}}(t)) \quad (25) $$

where, although ${}^H\boldsymbol{T}_R$ is calculated by $\boldsymbol{\psi}(t)$, it can also be measured by the on-line visual pose estimation method [17, 18]. In this study, it is assumed that the parameter $\boldsymbol{\psi}(t)$ was detected correctly. Here, the torque $\boldsymbol{\tau}_h(t)$ exerted on the driving motors of the humanoid in order to minimize $\delta\boldsymbol{\psi}(t) = \boldsymbol{\psi}_d(t) - \boldsymbol{\psi}(t)$ is calculated from ${}^H\boldsymbol{T}_{H_d}$, which is the pose deviation of the robot's head, caused by the influence of the gravity force and walking dynamics. The joint torque $\boldsymbol{\tau}_h(t)$, which pulls the robot's head up, is given by the following equation:

$$ \boldsymbol{\tau}_h(t) = \boldsymbol{J}_h(\boldsymbol{q})^T \boldsymbol{K}_p \delta\boldsymbol{\psi}(t), \quad \ldots\ldots\ldots (26) $$

where $\boldsymbol{J}_h(\boldsymbol{q})$ is a Jacobian matrix of the head pose against joint angles including q_1, q_2, q_3, q_4, q_9, q_{10}, q_{11}, q_{18}, which means that the joints from the supporting-foot to the head are included; $\boldsymbol{K}_p$ is the proportional gain similar to impedance control. This input is used in order to compensate for falling motions caused by gravity or dangerous and unpredictable slipping motion during all walking states. Notice that the input torque for non-holonomic joints, such as joint-1 (toe of supporting-foot), τ_{h_1} in $\boldsymbol{\tau}_h(t)$ in Eq. (26) needs to be set to zero since this is a free joint. Although $\delta\boldsymbol{\psi}(t)$ is capable of representing error with regard to humanoid position and orientation, only the position was utilized in this stage; therefore, $\boldsymbol{K}_p$ was set as $\boldsymbol{K}_p = diag[20, 290, 1100]^T$.

3.2. Foot and Body Motion Generator

In addition to $\boldsymbol{\tau}_h(t)$ in Eq. (26), two other kinds of input torques were used: $\boldsymbol{\tau}_t(t) = [0,\ \tau_{t2},\ \tau_{t3},\ 0,\ \tau_{t5},\ \tau_{t6},\ \tau_{t7},\ 0,\ \ldots,\ 0]^T$, was used in order to make the floating-foot and supporting-foot step forward; and $\boldsymbol{\tau}_w(t) = [0,\ \ldots,\ 0,\ \tau_{w8},\ 0,\ \ldots,\ 0]^T$, was used in order to swing the waist's roll angle (joint-8) for the purpose of realizing the arm swinging motion through dynamical coupling. The element $\boldsymbol{\tau}_t(t)$ and $\boldsymbol{\tau}_w(t)$ are shown below.

$$ \tau_{t2} = K_{p2}(q_{d2} - q_2) \quad \ldots\ldots\ldots (27) $$

$$ \tau_{t3} = K_{p3}(q_{d3} - q_3) \quad \ldots\ldots\ldots (28) $$

$$ \tau_{t5} = 20\cos\left[2\pi\frac{(t-t_2)}{1.85}\right] \quad \ldots\ldots\ldots (29) $$

$$ \tau_{t6} = K_{p6}(q_{d6} - q_6) \quad \ldots\ldots\ldots (30) $$

$$ \tau_{t7} = K_{p7}(q_{d7} - q_7) \quad \ldots\ldots\ldots (31) $$

$$ \tau_{w8} = 50\sin\left[2\pi\frac{(t-t_2)}{1.85}\right] \quad \ldots\ldots\ldots (32) $$

Here, t_2 represents the time when the supporting-foot and contacting-foot are switched. In the above equations, $q_{d2} = -0.2$ rad, $q_{d3} = 0.3$ rad, $q_{d6} = -0.5$ rad, $q_{d7} = 0.6$ rad are constant in order to make each joint angle change according to the desired values; $K_{p2} = 50$, $K_{p3} = 50$, $K_{p6} = 100$, $K_{p7} = 60$.

3.3. Combined Lifting/Swinging Controller

Combining the three torque generators expressed in Eqs. (26)–(32), a walking controller is created as $\boldsymbol{\tau}(t) = \boldsymbol{\tau}_h(t) + \boldsymbol{\tau}_t(t) + \boldsymbol{\tau}_w(t)$.

4. Simulation of Bipedal Walking

Simulations were conducted under an environment consisting of the sampling time set to 2.0×10^{-4} sec, the coefficient of friction between foot and ground considered as a static friction coefficient where $\mu_s = 1.0$, and viscous friction considered as $\mu_k = 0.7$. The proportional gain of the VLA was set as $\boldsymbol{K}_p = diag[20,\ 290,\ 1100]$; the target height of the head was set to $\boldsymbol{\psi}_d = [2.30\ \text{m},\ 0,\ 0]$.

With regard to the simulation environment, the software "Borland C++ Builder Professional Ver.5.0" was used to develop a simulation program; "OpenGL Ver.1.5.0" was used to display humanoid's time-transient configurations.

Figure 4 represents the position of the waist joint and center of gravity (COG) during the simulation of 100 walking steps. The upper part of **Fig. 4** shows a screenshot of the walking simulation. The A point represents the initial posture; B and B' show the state before and after the switching of the supporting-foot in the first step; C and C' show the second time of supporting-foot switching. The lower two columns show the transition of waist and COG from the transient responses to the stable state, described by the coordinate Σ_{toe}, which is fixed at the toe of the supporting-foot. The initial stage of walking occurs between the 1st and 5th steps, as depicted in **(b)** and **(c)**; the trajectories of both waist and COG do not converge. In these figures, points A, B, B', C and C' correspond to position profiles in **(a)**. The convergence stage occurs between the 6th step and 10th steps in **(d)** and **(e)**. At this stage, the various initial motion trajectories tend to converge. Finally, the stable stage is entered after the 10th step in **(f)** and **(g)**. At this stage, the waist trajectory and COG converge to a very narrow trajectory (almost one line).

Figure 5 shows the angle q_G between the COG and the origin of Σ_{toe}. The angle q_G is defined in **Fig. 1**, and can express the inclination of the body. **Fig. 5** shows the walking period T_1–T_4. In the initial stage (T_1 and T_2), q_G fluctuated in each step. In the third and fourth stage (T_3 and T_4), q_G started to become constant in each step. After T_4, the q_G was constant in each step.

Figures 6 and **7** represent the relationship of angle q_8 and waist joint angular velocity $\dot{q}_8$ during 100 steps, which indicates the stability of walking. **Fig. 6** shows the initial and convergence stage (from the 1st to the 10th step). In this stage, the movement of the waist is variable and does not converge to one trajectory. When entering

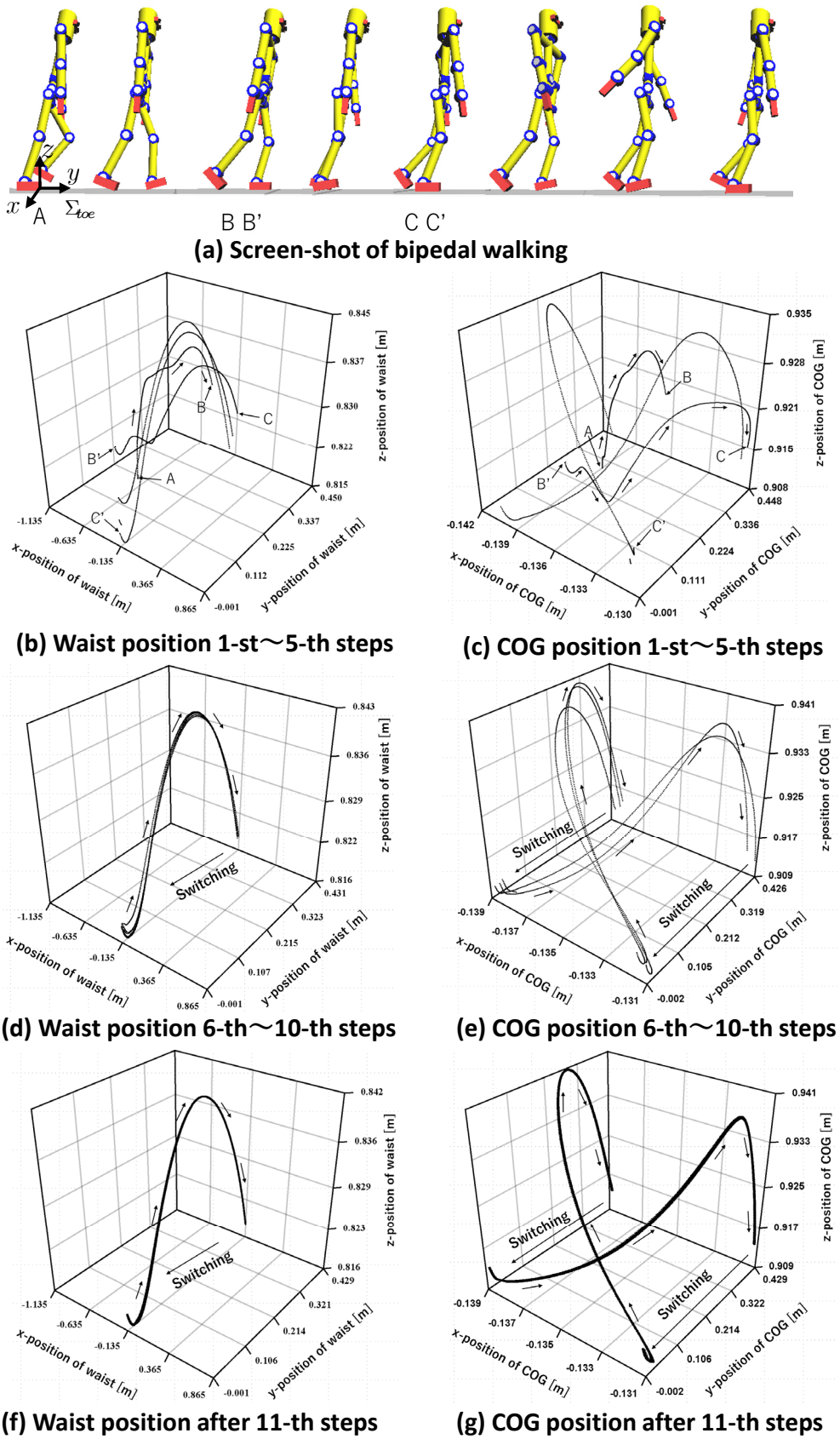

Fig. 4. Position of waist joint and COG during 100 steps walking simulation. The A point represents the initial posture; B and B' show the state before and after the switching of supporting-foot in the first step, respectively; C and C' show the second time of supporting-foot switching. There are three stages in the walking simulation. The initial stage is from 1st to 5th step; the convergence stage from 6th step to 10th step; stable stage occurs after the 10th step.

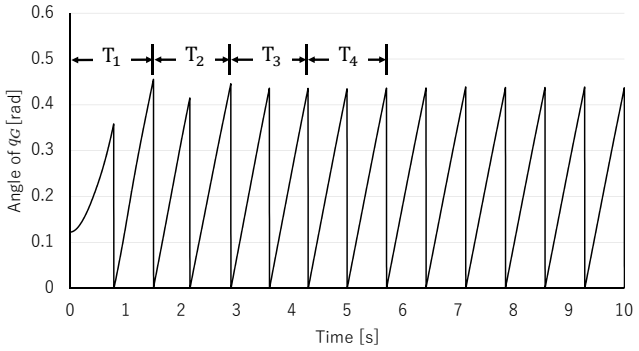

Fig. 5. Angle q_G between COG and origin point of world coordinate system Σ_W defined in **Fig. 1**.

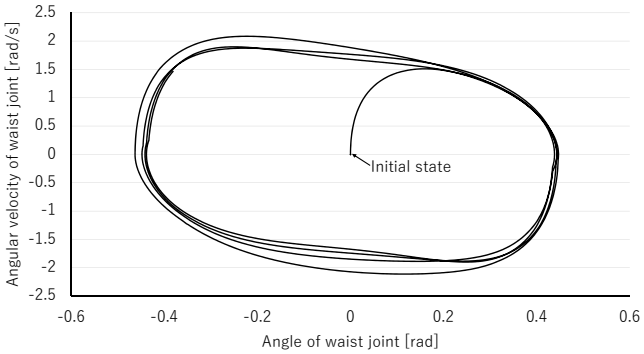

Fig. 6. Relation of angle q_8 and angular velocity $\dot{q}_8$ of waist joint in initial and convergence stage (from 1st to 10th step).

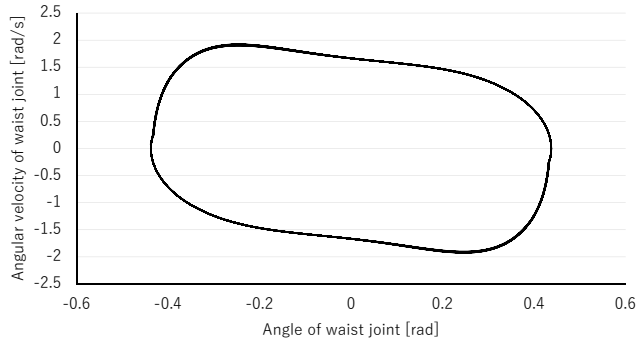

Fig. 7. Relation of angle q_8 and angular velocity $\dot{q}_8$ of waist joint in stable stage (after 11th step).

the steady state, shown in **Fig. 7**, the movement of the waist enters a limit cycle with very small width.

Figures 8 and **9** show the z-axis position (height) of the head, waist and knee (right), based on the world coordinate system Σ_W, during 100 steps of walking. As shown in **Fig. 8**, not only the movement of waist but also the head and knee oscillate steadily; it can be seen that the trajectory of motion is stable. **Fig. 9** is the expansion of **Fig. 8** in time. The height of the head, waist and knee, before falling in steady state walking, are depicted more precisely than in **Fig. 8**. After the 11th step, the walking motion profile seems to be the same as described in

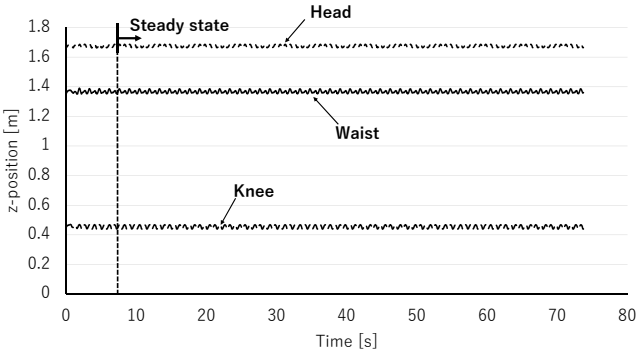

Fig. 8. z-axis position (height) of head, waist, knee (right) joint based on world coordinate system Σ_W during 100 steps walking simulation. After the 11th step comes the steady state as shown in the **Figs. 4(f)** and **(g)**.

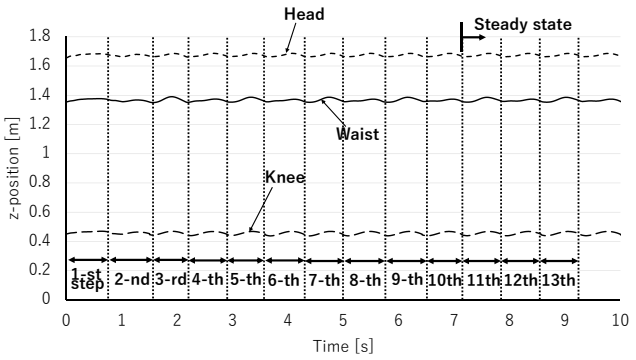

Fig. 9. z-axis position (height) of head, waist, knee (right) before steady state in **Fig. 8**. After 11th step, vibrational motion of head, waist and knee become stable.

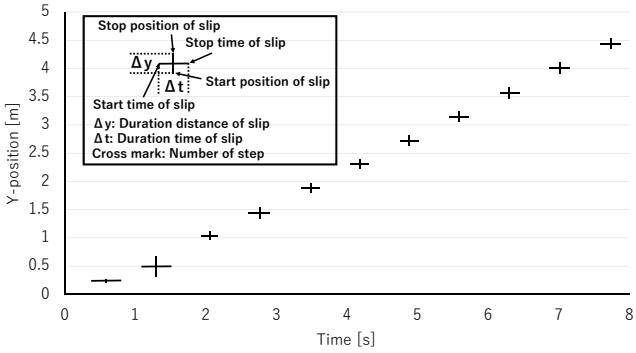

Fig. 10. Relationship between slip distance Δy (vertical bar) and slip time Δt (horizontal bar) of free-foot during 1st to 11th step.

Figs. 4(f) and **(g)**. The vibrational motion of the head, waist and knee become stable.

Figure 10 represents the free-foot's slip distance Δy and slipping duration Δt, from the initial stage until the stable walking. In the initial stage (1st to 5th step), both the distance and the time of slip change irregularly, such that $\Delta y_{1-5} = 0.003, 0.319, 0.109, 0.148, 0.116$ m, $\Delta t_{1-5} = 0.385, 0.388, 0.192, 0.266, 0.210$ s. From the convergence

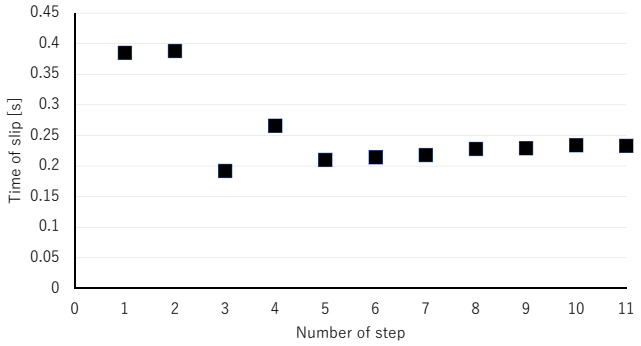

Fig. 11. Free-foot slip time Δt during 1st to 11th step and approximate curve representing the convergence state.

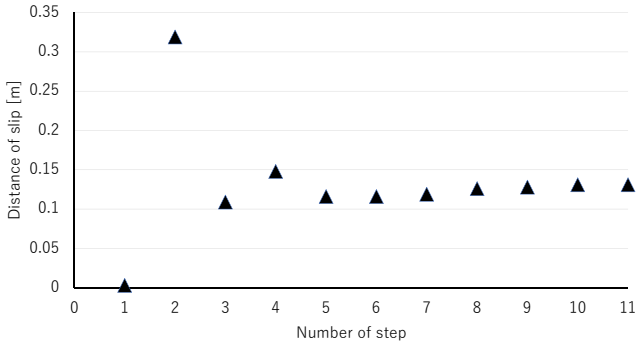

Fig. 12. Free-foot slip distance Δy during 1st to 11th step and approximate curve representing the convergence state.

stage to the steady state, both distance and time converge and become almost constant such that: $\Delta y_{6-11} = 0.116, 0.119, 0.126, 0.128, 0.131, 0.131$ m and $\Delta t_{6-11} = 0.214, 0.218, 0.228, 0.229, 0.234, 0.233$ s.

Figures 11 and **12** show the approximate curves of slip time Δt and slip distance Δy, of the slip which represents the convergence state. It follows from the figures that both the slip time and slip distance change greatly before the 5th step; after the 6th step, slip motion becomes stable.

5. Conclusion

As a first step in realizing human-like natural walking, this paper discussed humanoid walking using a two degree-of-freedom control combined with the Visual Lifting Approach (VLA) by feedforward and feedback and based on a dynamical model that contains flat feet including toe, slipping and impact. The simulation results confirmed that the combined strategy can help realize ZMP-independent stable walking. In future works, slipping phenomena in both lateral and rotational directions, around the vertical axis should be considered. Then, in order to verify the validity of the proposed method, the noise and perturbation in the humanoid model will be considered, in addition to preventing or utilizing slippage.

References:

[1] M. Vukobratovic, A. Frank, and D. Juricic, "On the Stability of Biped Locomotion," IEEE Trans. on Biomedical Engineering, Vol.17, No.1, 1970.

[2] M. Vukobratovic and J. Stepanenko, "On the Stability of Anthropomorphic Systems," Mathematical Biosciences, Vol.15, pp. 1-37, 1972.

[3] S. Colins, A. Ruina, R. Tedrake, and M. Wisse, "Efficient Bipedal Robots Based on Passive-Dynamic Walkers," Science, Vol.307, pp. 1082-1085, 2005.

[4] J. Pratt, P. Dilworth, and G. Pratt, "Virtual Model Control of a Bipedal Walking Robot," Proc. of IEEE Int. Conf. on Robotics and Automation," pp. 193-198, 1997.

[5] R. E. Westervelt, W. J. Grizzle, and E. D. Koditschek, "Hybrid Zero Dynamics of Planar Biped Walkers," IEEE Trans. on Automatic Control, Vol.48, No.1, pp. 42-56, 2003.

[6] Y. Harada, J. Takahashi, D. Nenchev, and D. Sato, "Limit Cycle Based Walk of a Powered 7DOF 3D Biped with Flat Feet," Proc. of IEEE/RSJ Int. Conf. on Intelligent Robots and Systems, pp. 3623-3628, 2010.

[7] Y. Huang, B. Chen, Q. Wang, K. Wei, and L. Wang, "Energetic efficiency and stability of dynamic bipedal walking gaits with different step lengths," Proc. of IEEE/RSJ Int. Conf. on Intelligent Robots and Systems, pp. 4077-4082, 2010.

[8] D. Peng and K. G. Shin, "Modeling of Concurrent Task Execution in a Distributed System for Real-Time Control," IEEE Trans. on Computers, Vol.C-36, No.4, pp. 510-516, April 1987.

[9] T. Wu, T. Yeh, and B. Hsu, "Trajectory Planning of a One-Legged Robot Performing Stable Hop," Proc. of IEEE/RSJ Int. Conf. on Intelligent Robots and Systems, pp. 4922-4927, 2010.

[10] Y. Nakamura and K. Yamane, "Dynamics of Kinematic Chains with Discontinuous Changes of Constraints – Application to Human Figures that Move in Contact with the Environments –," J. of RSJ, Vol.18, No.3, pp. 435-443, 2000 (in Japanese).

[11] K. Yamane and Y. Nakamura, "Dynamics Filter – Concept and Implementation of On-Line Motion Generator for Human Figures," IEEE Trans. on Robotics and Automation, Vol.19, No.3, pp. 421-432, 2003.

[12] X. Li, H. Imanishi, M. Minami, T. Matsuno, and A. Yanou, "Dynamical Model of Walking Transition Considering Nonlinear Friction with Floor," J. of Advanced Computational Intelligence and Intelligent Informatics, Vol.20, No.6, 2016.

[13] W. Song, M. Minami, and Y. Zhang, "A Visual Lifting Approach for Dynamic Bipedal Walking," Int. J. of Advanced Robotic Systems, Vol.9, pp. 1-8, 2012.

[14] A. Yanou, M. Minami, T. Maeba, and Y. Kobayashi, "A First Step of Humanoid's Walking by Two Degree-of-freedom Generalized Predictive Control Combined with Visual Lifting Stabilization," Proc. of the 39th Annual Conf. of the IEEE Industrial Electronics Society (IECON2013), pp. 6357-6362, 2013.

[15] W. Song, M. Minami, T. Maeba, Y. Zhang, and A. Yanou, "Visual Lifting Stabilization of Dynamic Bipedal Walking," Proc. of 2011 IEEE-RAS Int. Conf. on Humanoid Robots, pp. 345-351, 2011.

[16] N. Hogan, "Impedance Control; An Approach to Manipulation, Parts I–III," ASME J. of Dynamics Systems, Measurement, and Control Vol.107, No.1, pp. 1-24, 1985.

[17] W. Song, M. Minami, F. Yu, Y. Zhang, and A. Yanou, "3-D Hand & Eye-Vergence Approaching Visual Servoing with Lyapunov-Stable Pose Tracking," Proc. of IEEE Int. Conf. on Robotics and Automation, pp. 5210-5217, 2011.

[18] F. Yu, W. Song, and M. Minami, "Visual Servoing with Quick Eye-Vergence to Enhance Trackability and Stability," Proc. of IEEE/RSJ Int. Conf. on Intelligent Robots and Systems, pp. 6228-6233, 2010.

[19] M. Kouchi, M. Mochimaru, H. Iwasawa, and S. Mitani, "Anthropometric database for Japanese Population 1997-98," Japanese Industrial Standards Center (AIST, MITI), 2000.

[20] T. Maeba, M. Minami, A. Yanou, and J. Nishiguchi, "Dynamical Analyses of Humanoid's Walking by Visual Lifting Stabilization Based on Event-driven State Transition," 2012 IEEE/ASME Int. Conf. on Advanced Intelligent Mechatronics Proc., pp. 7-14, 2012.

Name:
Xiang Li

Affiliation:
Ph.D. Student, Graduate School of Natural Science and Technology, Okayama University

Address:
3-1-1 Tsushima-naka, Okayama 700-8530, Japan

Brief Biographical History:
2014- Master Course Student, Graduate School of Natural Science and Technology, Okayama University
2016- Ph.D. Student, Graduate School of Natural Science and Technology, Okayama University

Main Works:
• "Dynamical Model of Walking Transition Considering Nonlinear Friction with Floor," J. of Advanced Computational Intelligence and Intelligent Informatics, Vol.20, No.6, 2016.
• "Dynamic Reconfiguration Manipulability for Redundant Manipulators," J. of Mechanisms and Robotics, Vol.8, December 2016.

Membership in Academic Societies:
• The Institute of Electrical and Electronics Engineers (IEEE)
• The Society of Instrument and Control Engineers (SICE)
• The Robotics Society of Japan (RSJ)

Name:
Mamoru Minami

Affiliation:
Professor, Graduate School of Natural Science and Technology, Okayama University

Address:
3-1-1 Tsushima-naka, Okayama 700-8530, Japan

Brief Biographical History:
1990- Doctoral Course Student, Graduate School of Natural Science and Technology, Kanazawa University
1994- Associate Professor, Department of Mechanical Engineering, University of Fukui
2002- Professor, Department of Human and Artificial Intelligence Systems, University of Fukui
2010- Professor, Graduate School of Natural Science and Technology, Okayama University

Main Works:
• "Reconfiguration Manipulability Analyses for Redundant Robots," Trans. of the ASME, J. of Mechanisms and Robotics, Vol.5, No.4, pp. 1-16, 2013.
• "Visual Servoing to catch fish Using Global/local GA Search," IEEE/ASME Trans. on Mechatronics, Vol.10, No.3, pp. 352-357, 2005.

Membership in Academic Societies:
• The Institute of Electrical and Electronics Engineers (IEEE)
• The Japanese Society of Mechanical Engineers (JSME)
• The Society of Instrument and Control Engineers (SICE)
• The Robotics Society of Japan (RSJ)

Name:
Takayuki Matsuno

Affiliation:
Associate Professor, Graduate School of Natural Science and Technology, Okayama University

Address:
3-1-1 Tsushima-naka, Okayama 700-8530, Japan

Brief Biographical History:
2000 Received M.E. degree from Nagoya University
2005 Received Dr.Eng. from Nagoya University
2004- Joined Nagoya University
2006- Joined Toyama Prefectural University

Main Works:
• "Manipulation of Deformable Linear Objects using Knot Invariants to Classify the Object Condition Based on Image Sensor Information," IEEE/ASME Trans. on Mechatronics, Vol.11, Issue 4, pp. 401-408, 2006.
• "Development of Production Robot System that can Assemble Products with Cable and Connector," J. of Robotics and Mechatronics, Vol.23, No.6, pp. 939-950. 2011.

Membership in Academic Societies:
• The Institute of Electrical and Electronics Engineers (IEEE) Robotics and Automation Society (RAS)
• The Japan Society of Mechanical Engineers (JSME)
• The Robotics Society of Japan (RSJ)
• The Society of Instrument and Control Engineers (SICE)

Name:
Daiji Izawa

Affiliation:
Master Course Student, Graduate School of Natural Science and Technology, Okayama University

Address:
3-1-1 Tsushima-naka, Okayama 700-8530, Japan

Brief Biographical History:
2016- Master Course Student, Graduate School of Natural Science and Technology, Okayama University

Main Works:
• "Verification of Humanoid Robot Model Considering Stick/Slip Friction," 22nd Int. Symposium on Artificial Life and Robotics, January 18-20, 2017.